Continuous accumulation of cold atoms in an optical cavity

Edward Gheorghita,[*] Sebastian Wald,[*] Andrea Pupić, and Onur Hosten[†]
Institute of Science and Technology Austria (ISTA), 3400 Klosterneuburg, Austria

(Received 16 December 2025; accepted 13 July 2026; published 3 August 2026)

Continuously operating atom-light interfaces represent a key prerequisite for steady-state quantum sensors and efficient quantum processors. Here, we demonstrate continuous accumulation of sub-Doppler-cooled atoms in a shallow intracavity dipole trap, realizing this regime. The key ingredient is a light-shift manipulation that creates spatially varying cooling parameters, enabling efficient capture and accumulation of atoms within a cavity mode. Demonstrated with rubidium atoms, a continuous flux from a source cell is funneled through the magneto-optical trap into the cavity mode, where the atoms are cooled and maintained below 10 μK in steady state without time-sequenced operation. We characterize the resulting continuously maintained ensemble of millions of atoms and its collective coupling to the cavity field, establishing a route toward continuously operated cavity-QED systems and long-duration atomic and hybrid quantum sensors.

DOI: 10.1103/71f2-sq4p

I. INTRODUCTION

Continuous atom-light interfaces represent an important frontier for realizing quantum systems capable of uninterrupted sensing and efficient information processing. In such systems, the atomic and optical degrees of freedom can remain coherently coupled in steady state. Substantial progress has been made toward this goal in a range of platforms, including cavity-based quantum interfaces [1–7]. However, achieving simultaneous atom loading, cooling, and confinement within an optical cavity remains a central experimental challenge due to conflicting requirements. The same light fields that provide trapping typically inhibit sub-Doppler cooling, preventing continuous accumulation of atoms. Consequently, such interfaces still rely on time-sequenced operation, alternating between loading, cooling, and interrogation phases.

Here, we demonstrate a method to overcome this challenge, continuously accumulating and cooling atoms directly within the mode of an optical cavity without time sequencing. This allows for maintaining a steady-state population of atoms continuously coupled to the cavity field, able to perform continuous interrogation. The key is a light-shift-manipulation technique that simultaneously allows capturing, cooling, and maintaining atoms in the same spatial region. Specifically, working with ^{87}Rb atoms, we use a two-tone trap formed primarily by 1560-nm light with a small 1527-nm contribution. This configuration enables a simultaneous operation of a magneto-optical trap, a dipole trap, and optical molasses. Atoms are continuously transferred from the source to the magneto-optical trap (MOT) and then to the dipole trap. The required laser detunings for sub-Doppler cooling are naturally provided by the position-dependent energy shifts induced by the two-tone trap. In the process, several million atoms can accumulate in steady state, decoupled from the cooling light inside the trap, at temperatures that can reach 5 μK.

In a recent work, continuous atom-cavity coupling was achieved by cooling on a narrow optical transition and by employing spatially separated regions for cooling and coupling [2]. In contrast, our approach uses broad-line laser cooling to realize continuous loading and steady-state accumulation directly within the cavity mode, without relying on the naturally low temperatures available in narrow-line species.

The ability to sustain a steady-state ensemble of atoms within an optical cavity opens the way to novel and improved quantum protocols across a broad range of systems. These include continuous-wave active atomic clocks [8], the possibility of steady-state operation for the emerging hybrid cold atom-optomechanical quantum systems [9], and efficient reloading of atoms into a quantum processor for running large-scale error-corrected quantum computations [10].

II. CONTEXTUAL SETTING

The setup utilized for this work was designed to explore entanglement-enhanced sensing [12,13], with an emphasis on generating spin-squeezed states [14–18], enhancing [19–21] atom interferometric inertial sensors [22–25], and improving the performance of cavity-based atomic clocks [26,27]. At the core of the setup (see Appendix A) is an in-vacuum traveling-wave optical cavity [Fig. 1(a)]. The mirrors for the cavity are coated for operation near both 780 nm and 1560 nm, with low- and high-finesse modes for two orthogonal linear polarizations for each wavelength. The 780-nm modes interact with the atoms near-resonantly, while the 1560-nm modes form a far off-resonant dipole trap for the atoms. A three-dimensional (3D) MOT is nearly overlaid with the cavity mode waist to

[*]These authors contributed equally to this work.
[†]Contact author: onur.hosten@ist.ac.at

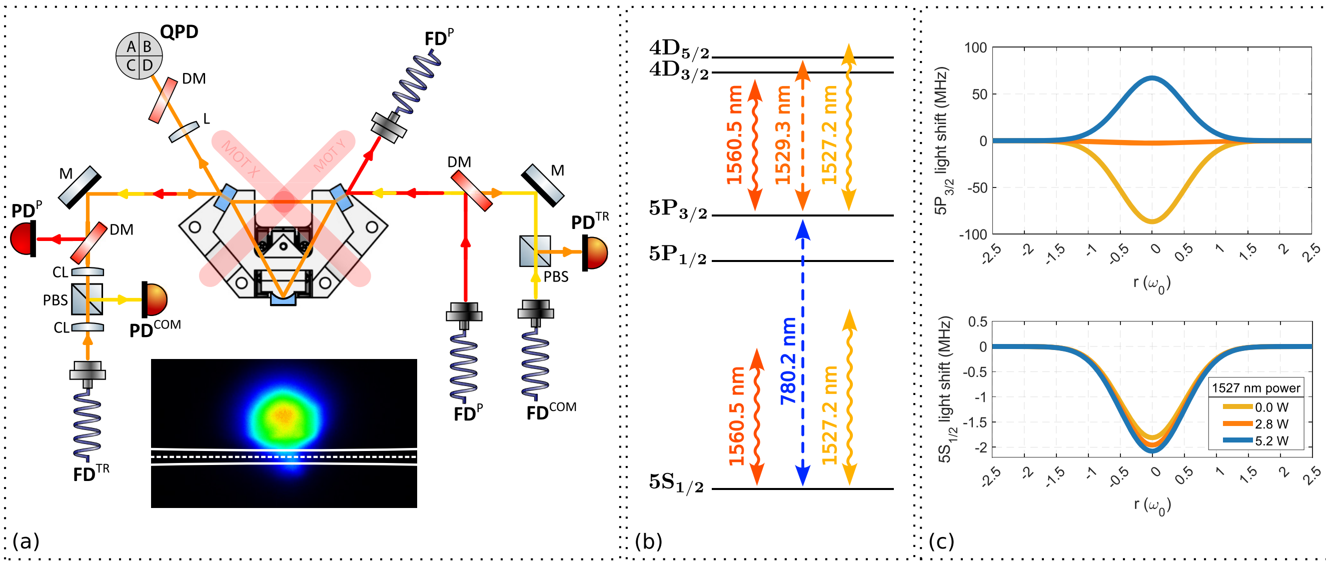

FIG. 1. (a) Schematic of the traveling-wave cavity and the light tones coupled to the cavity formed by three mirrors (blue) attached to a monolithic spacer. The superscripts TR, COM, and P refer to the trapping, compensation, and cavity probe tones, respectively. The 1560-nm trap tone is frequency locked to a high-finesse cavity mode via the squash-locking method [11] utilizing a quadrant photodiode (QPD) in reflection and the 780-nm probe tone is generated via frequency doubling. FD: fiber dock, PD: photodiode, M: mirror, DM: dichoric mirror, PBS: polarizing beam splitter, CL: cylindrical lens, L: spherical lens. Inset: Illustration of the geometry, where atoms are "*sipped*" into the cavity mode (solid and dashed lines) from the edge of the 500-µm $1/e^2$-radius MOT, imaged here through its fluorescence in absence of the compensation tone. (b) Energy diagram for ^{87}Rb, illustrating the relevant transition wavelengths (dashed) in connection with the applied tones. (c) Illustration of the total light-induced energy level shifts in the ground and excited states for three different 1527-nm intravacity powers for 157-µm beam waist and 36-W intracavity 1560-nm power.

load atoms from a commercial two-dimensional (2D)-MOT-based atom source.

The 780/1560-nm dual-wavelength configuration offers both technical and fundamental advantages. It benefits from the low-noise infrastructure available in the telecom band around 1560 nm; allows streamlined frequency locking, in which a cavity-locked 1560-nm trap beam renders its frequency-doubled 780-nm tone resonant with the cavity; and enables uniform atom-cavity coupling in a standing-wave geometry [17]. Despite these desirable features, a 1560-nm tone rather strongly couples the 1529-nm $5P_{3/2} \leftrightarrow 4D$ transitions of rubidium [Fig. 1(b)]. This coupling induces spatially varying light shifts on the $5P_{3/2}$ excited states with a magnitude nearly 50 times those for the $5S_{1/2}$ ground states [Fig. 1(c)]. This mismatch in light shifts poses challenges for operating a MOT, transferring atoms from the MOT to the dipole trap, and further executing well-established cooling techniques.

Overcoming these challenges has been a subject of investigation. The most straightforward operation for further cooling inside a 1560-nm dipole trap was to intermittently switch off the dipole trap [28]. To improve loading efficiency into these traps, a narrow-resonance dark-state cooling method was investigated, nearing an order of magnitude improvement in the number of trapped atoms—reaching 1%–2% MOT-to-dipole trap transfer efficiencies and 200-µK in-trap temperatures [29,30]. Building on the light-shift engineering ideas of Ref. [31] for loading cold atoms into deep dipole traps, adding an auxiliary 1529-nm tone to a free-space 1560-nm dipole trap was shown to increase trapped atom numbers—reaching 7% MOT-to-dipole-trap transfer efficiency and 50-µK in-trap temperatures [32,33]. Related 1529-nm light-shift control has also been employed to improve the uniformity of nondestructive atomic-state probing [34,35] and to spectrally hide atoms during state manipulations in optical tweezer arrays [36].

As we demonstrate here, light-shift compensation can not only improve transfer efficiencies and cooling beyond what has been shown, but can enable a conceptually distinct steady-state accumulation of atoms in a time-independent trap without interfering with atomic-state control. We emphasize that this effect does not rely on the accidental strong coupling of the trapping tone to higher-lying levels in rubidium, but is instead generally applicable to arbitrary atomic species and to dipole traps at other wavelengths.

In our setup, a weak 1527-nm tone is used for light-shift compensation. This tone is frequency locked to a low-finesse cavity mode with the side-of-fringe technique [37] to directly stabilize its intracavity optical power. The cavity modes at 1527 nm share essentia lly the same characteristics as those at 1560 nm. Due to the power enhancement provided by the cavity, we only work with milliwatts of light for both tones, which turn into several watts inside the cavity.

III. CONTROL OF LIGHT SHIFTS

The light shift of the $5P_{3/2}$ level is selectively controlled by varying the power of the auxiliary 1527-nm traveling-wave tone. In terms of the frequency-dependent scalar polarizability α_i, the shift for level i can be expressed as $\Delta E_i = -\frac{1}{2}\alpha_i \mathcal{E}_{\rm rms}^2$, where $\mathcal{E}_{\rm rms}$ is the position-dependent root-mean-square electric field of a single light tone [38,39]. Due to the opposite detunings of the 1560- and 1527-nm tones for this transition, the corresponding polarizabilities carry opposite signs

TABLE I. Calculated scalar polarizabilities α_i in units (J)(m^2)/(W). For $5S_{1/2}$, we include the contribution from the $5S_{1/2} \rightarrow (5P_{3/2}, 5P_{1/2})$ transitions. For $5P_{3/2}$, we include the contribution from the $5P_{3/2} \rightarrow (6S_{1/2}, 4D_{1/2}, 4D_{5/2})$ transitions [39].

λ (nm)	$\alpha_{5S_{1/2}}$	$\alpha_{5P_{3/2}}$
1560	6.804×10^{-39}	3.259×10^{-37}
1527	6.906×10^{-39}	-3.928×10^{-36}

(Table I). Achieving a net-zero light shift on the $5P_{3/2}$ levels requires satisfying an intensity ratio of $I_{1527} = \frac{1}{12.1} I_{1560}$. In Fig. 1(c), we show the calculated light shifts across the dipole trap for three intensity ratios, using the intensity relation $I = \epsilon_0 c \mathcal{E}_{\rm rms}^2$.

Atoms confined in the dipole trap experience light shifts in both the ground ($5S_{1/2}$) and the excited ($5P_{3/2}$) states. A probe beam coupling these levels, with a scanned detuning, enables measurement of the differential light shift $\delta = \Delta E_{5P_{3/2}} - \Delta E_{5S_{1/2}}$ via the resulting fluorescence signal [40,41]. In our implementation, the 780-nm MOT cooling beams that couple the $F = 2$ hyperfine manifold of the ground states to the $F' = 3$ hyperfine manifold of the excited states [42] act as the probe, enabling characterization of light shifts for different compensation powers (Fig. 2). During these 300-μs measurements, trapping and compensation beams stay on, and an additional 780-nm repump beam with a detuning optimized for each compensation power returns atoms that have decayed into the $F = 1$ ground hyperfine manifold back into $F = 2$. The probe operates at around one saturation intensity, yielding a 10-MHz full width for the fluorescence spectrum in absence of trap and compensation beams—smaller than the widths of the distributions in Fig. 2. The mean shifts obtained for the three compensation powers demonstrate that we can shift the excited state levels to either direction in frequency in comparison to their natural values. The chosen intermediate compensation power cancels the mean differential shift caused by the trap.

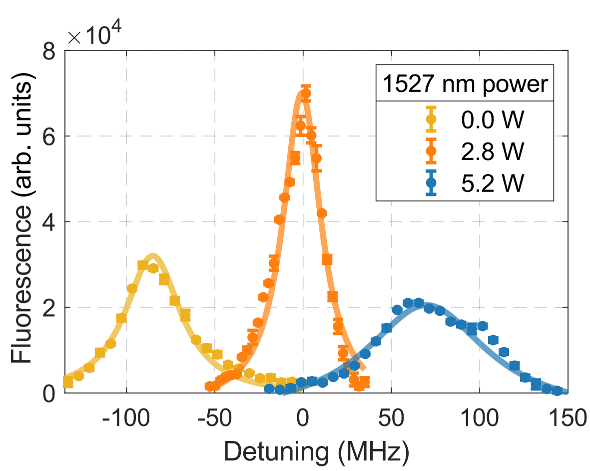

FIG. 2. Characterization of light-shift distributions for the $F = 2 \rightarrow F' = 3$ transition for three different 1527-nm intracavity powers: no compensation (yellow), full compensation (orange), and overcompensation (blue). The 1560-nm intracavity power is fixed at 36 W.

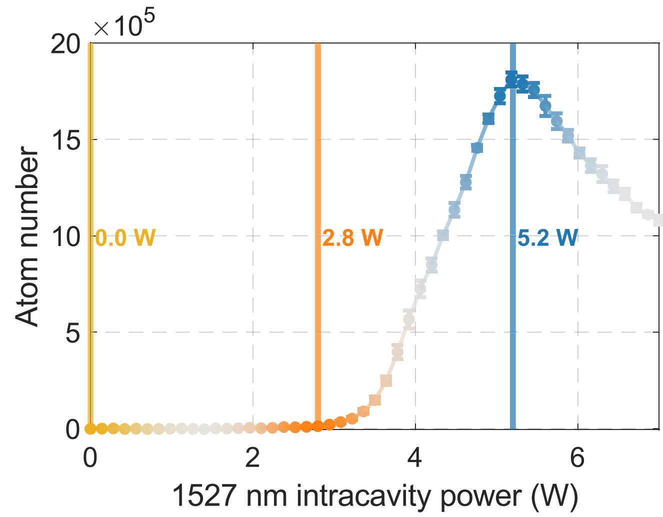

FIG. 3. Number of accumulated atoms in the dipole trap after a 550-ms accumulation time as a function of compensation tone power. Three specific compensation levels associated with regions with qualitatively different behaviors are highlighted.

For a discussion on the widths of the light-shift distributions and potential role of tensor polarizability see Appendix B.

IV. CONTINUOUS ACCUMULATION

For a given dipole trap depth, beyond a threshold compensation power, we observe that atoms naturally start accumulating inside the dipole trap concurrently with MOT loading. The efficiency of this transfer does *not* seem to depend critically on a good spatial overlap between the MOT and the cavity mode, as loading through the edge of the MOT [Fig. 1(a), inset] and through its center yields similar results.

The number of atoms loaded into a 87-μK-deep (36 W) dipole trap is demonstrated in Fig. 3 as a function of the 1527-nm intracavity power for an accumulation duration of 550 ms. For reference, we highlight the three specific powers corresponding to the light shifts indicated and studied in Figs. 1(c) and 2. First, in the absence of a compensation tone, the light shift from the 1560 nm locally inhibits the operation of the MOT. In this configuration, a MOT overlapped with the cavity mode can even fail to load atoms at sufficiently high trap powers. Next, at around 2.8 W in the compensation tone, while the MOT loads virtually unimpeded, no atoms are loaded into the dipole trap. Although this power corresponds to the intensity ratio at which the light shift is optimally compensated, the atomic temperatures in the MOT are too high to retain them in the utilized trap depth. Finally, for larger compensation powers (effectively red-detuning the cooling light for the atoms), a sharp rise in the number of atoms in the dipole trap is observed, reaching values as large as 1.8×10^6. This is 63% of the full 2.9×10^6 atoms accumulated in the dipole trap in steady state for this configuration.

These experiments begin by switching on the MOT coils as well as the cooling and repumper beams (5 mW/cm^2 per cooling beam, 180 μW/cm^2 repumper) and setting a 1527-nm intracavity power. After 550 ms, the cooling and repumper beams and coils are turned off. Atoms are kept in the trap

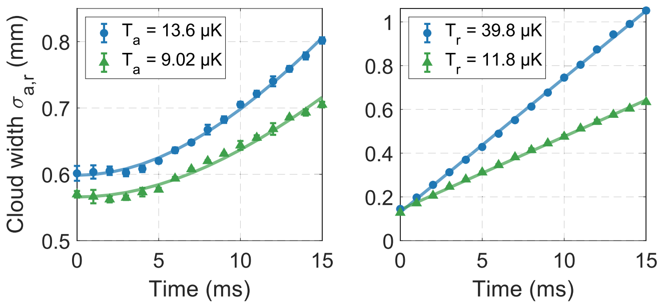

FIG. 4. Measured temperature of the atoms in the axial "a" and radial "r" directions, characterized by a time-of-flight measurement. Blue circles: Measurements after continuous accumulation. The 1560-nm and 1527-nm intracavity powers were 36 and 5.2 W, respectively, throughout accumulation and storage. Green triangles: After accumulation, the 1527 nm is set to 2.8 W and optical molasses is applied for 10 ms.

for another 100 ms before they are released from the trap for fluorescence imaging with a resonant pulse.

A key feature enabling continuous accumulation is the presence of natural sub-Doppler cooling. We characterize this with standard time-of-flight measurements [43] (Fig. 4, upper curves). In the axial trapping direction we measure temperatures as low as 13 μK, while in the radial direction we obtain temperatures of 40 μK. Although we do not have a model for this temperature asymmetry, the culprit is the difference in trap frequencies between the two directions; 185 Hz and 0.41 Hz, respectively. For the extraction of temperatures, we fit the time-dependent standard deviation $\sigma(t) = (\sigma_0^2 + k_B T t^2/m)^{1/2}$ for the expanding clouds, with temperature T and initial width σ_0 as fit parameters; m: ^{87}Rb atomic mass, k_B: Boltzmann constant.

The processes in effect for accumulation and cooling can be understood intuitively. Although the MOT beams are red-detuned by 2.5 Γ outside of the trap, with the compensation power set to 5.2 W, atoms in the trap are light shifted by 69 MHz on average (see Fig. 2), experiencing a red detuning of 14 Γ. Thus, as the atoms captured by the MOT near the edge of the trapping potential move toward the center of the dipole trap, they experience increasingly red-detuned cooling light, starting to undergo polarization gradient cooling [44]. However, instead of this being the standard time-sequenced operation, here it is position dependent. Simultaneous MOT capturing and spatially dependent far-detuned cooling reduce the motional energy below the dipole-trap depth, allowing them to be captured in a rather shallow dipole potential. Additional measurements reveal that in steady state, 85% of the atoms reside in the $F = 1$ manifold, providing further insight: Once the atoms are captured by the dipole trap, they undergo limited cycles of cooling within the $F = 2$ manifold. As they move toward the trap center, the repumper becomes off-resonant, and atoms that fall into the $F = 1$ manifold are stored in the trap, remaining isolated from the cooling light.

V. EXTENSIONS

We draw attention to the remarkably low levels of the required dipole trap depths to capture the atoms. For example,

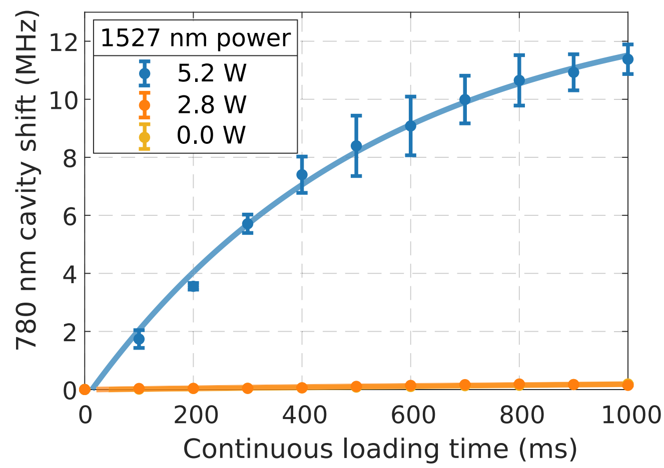

FIG. 5. Measured cavity resonance shift for the high-finesse 780-nm mode throughout the continuous accumulation process for different light-shift compensation levels. Yellow and orange curves are practically indistinguishable. For reference, the full width of the cavity resonance is 85 kHz.

in Ref. [28], at least 10 times deeper traps were required to retain a similar number of atoms. In Appendix D, we discuss accumulation in even shallower traps, reaching temperatures of 3 μK, and a modified protocol that employs a nonstatic compensation power capable of additional enhancements in the loading efficiency.

Additionally, we highlight that the observed nonisotropic temperatures can be eliminated postaccumulation by further polarization gradient cooling under optimal light-shift compensation. This is demonstrated by the bottom curves in Fig. 4. Here, after accumulation, we set the compensation power to 2.8 W to cancel the light shifts and run the cooling for 10 ms in zero magnetic field (−20 Γ detuning, 0.8 mW/cm^2 per beam cooling, and 180 μW/cm^2 resonant repump). This suggests that isotropic distributions may also be achievable during continuous accumulation.

VI. CONTINUOUS STRONG CAVITY COUPLING

The accumulated atomic ensemble is continuously coupled to the cavity in the strong collective coupling regime during the described protocols, reaching collective cooperativities of order 10^5 (see Appendix C). Such a system can, for example, show continuous vacuum Rabi splitting [2]. Here, we use this continuous coupling in the dispersive regime to observe *in situ* the atom accumulation in the cavity mode.

Taking into account that the majority of the atoms in the cavity mode are in a specific hyperfine manifold F, the total cavity resonance shifts roughly measure the number of atoms in the cavity mode, with around 2 Hz/atom cavity shift (see Appendix C). Given their spatially selective and nondestructive nature, these measurements can be inserted at any instant during atom accumulation by scanning the cavity probe beam across the expected resonance. This removes the need to hold atoms in the dipole trap while waiting for surrounding MOT atoms to fall before measurements, as was required for fluorescence imaging. Figure 5 shows the cavity shifts observed during accumulation of the atoms for the three specific compensation tone powers, starting with no atoms in the system. The accumulation of atoms toward a steady-state value is clearly seen in the case with the high compensation level. In contrast, for the other two cases, where no atoms remain in the cavity mode, the cavity shifts are much smaller, attaining a relative magnitude of no more than 0.5%. These residual cavity shifts can then be attributed to the MOT atoms transiting the cavity.

VII. DISCUSSION

Beyond enabling continuous atom-light interfaces, the demonstrated light-shift compensation and continuous loading offer versatile operation for atom-cavity experiments. It becomes possible to perform quantum protocols with static intracavity trapping powers, eliminating the need to ramp trap powers between experimental cycles. This capability is particularly valuable for high-precision sensing, as it allows the cavity mirrors to reach a thermal steady state and suppresses heating-induced drifts of the cavity resonance. At the same time, the light-shift compensation enables seamless implementation of in-trap molasses cooling, optical pumping for internal-state preparation, and state-dependent removal of atoms from the dipole trap with a resonant push beam. The removal process enables efficient state purification or background measurements with atoms easily ejected. All these processes require more considerations and tradeoffs in absence of light-shift compensation.

Our results establish a operational regime in which laser cooling, optical trapping, and cavity coupling coexist seamlessly in steady state. The demonstrated light-shift-manipulation technique reconciles these normally competing requirements, enabling a stable ensemble of cold atoms to remain continuously coupled to the cavity field. This capability provides the essential experimental ingredient for continuous cavity QED with cold atoms. Because the method relies only on tunable optical parameters, conventional broadline transitions, and very shallow dipole traps, it can be readily adapted to a range of systems. This advance in continuous atom-light interfaces opens different prospects for continuous atomic quantum sensors and hybrid quantum platforms, and offers a path to continuously reloaded atomic quantum processors.

ACKNOWLEDGMENTS

The authors thank Vyacheslav Li for his earlier contributions to the development of the setup utilized in this work. This work was supported by the Institute of Science and Technology Austria (ISTA); E.G. was supported by the European Research Council under Grant No. 101087907 (ERC CoG QuHAMP).

DATA AVAILABILITY

There are no publicly available research data or software supporting this manuscript. Requests for further information or data should be sent to the authors.

APPENDIX A: EXPERIMENTAL SETUP

The optical cavity in the setup was designed with an aim to perform atom interferometry inside the cavity mode with spin-squeezed states and consequently has a number of particular properties: The traveling-wave nature of the cavity is (1) to ensure that the atoms are free to move along the cavity axis in the region of the cavity mode waist and (2) to be able to drive two-photon Raman transitions at 780 nm with counterpropagating beams to impart state-dependent momentum kicks along the cavity mode. The 3.05-GHz free-spectral-range traveling-wave cavity is formed by three mirrors in the plane-plane-convex configuration. The mirrors are coated for operation near both 780 and 1560 nm. The convex mirror is mounted on an ultrahigh-vacuum compatible piezo-based translation stage (SmarAct) to allow for in-vacuum fine tuning of the cavity length (Fig. 1). This enables simultaneous accommodation of two 780-nm intracavity tones separated by the 6.834-GHz hyperfine splitting of the ^{87}Rb atoms to drive the Raman transitions. Because the intracavity light undergoes reflections at nonnormal incidence, the two polarizations can acquire distinct characteristics. The coatings are optimized to form a high-finesse cavity for the out-of-plane polarization modes ($\mathcal{F}_{780}^{\text{high}} = 39 \times 10^3$ and $\mathcal{F}_{1560}^{\text{high}} = 103 \times 10^3$) while maintaining as low a finesse as possible for the in-plane polarization modes ($\mathcal{F}_{780}^{\text{low}} = 2.2 \times 10^3$ and $\mathcal{F}_{1560}^{\text{low}} = 30 \times 10^3$).

For additional information on cavity parameters, laser systems, and additional peripheral components of the system, see Appendixes E–H.

APPENDIX B: LIGHT SHIFTS

In the main text, level shifts due to interactions with linearly polarized far-off-resonant light have been treated utilizing *scalar* polarizabilities. In this approximation, all magnetic sublevels associated with a hyperfine level experience identical shifts. However, it is well know that *tensor* polarizabilities lift this degeneracy [38,45], resulting in a spread of sublevel shifts [41], which can even become nonperturbatively large for light with small detunings [32]. Depending on the relative polarizations of the trap and compensation lights, a compensation of the scalar shifts need not indicate a compensation of the tensor part, raising the question of to what extent the tensor shifts might interfere with laser cooling. A numerical analysis (using the code provided in Ref. [32]) for orthogonal linearly polarized trap and compensation lights shows that, in this configuration, the tensor shifts indeed do not cancel (Fig. 6) and always lift the degeneracy of the $5P_{3/2}$, $F' = 3$ magnetic sublevels: A full sublevel spread of 25, 40, and 55 MHz for the zero-, intermediate- and high-compensation powers utilized in the main text. Note that this analysis does not take into account the spread in the light shifts due to the spatial distribution of the atoms in the dipole trap at finite temperatures.

Spectral shapes associated with light-shift distributions in dipole traps have been studied in various configurations [32,41]. For our purposes, simple Lorentzian fits prove sufficient to extract approximate full widths yielding 40, 25, and 80 MHz for the zero,, intermediate-, and high-compensation levels for the distributions in Fig. 2. Note that these distributions are measured for atoms at 11 μK in both axial and

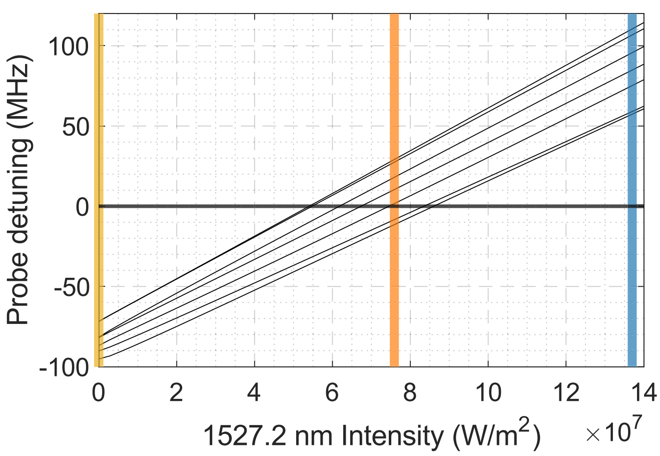

FIG. 6. Numerical calculation of light shifts for the magnetic sublevels of the $5P_{3/2}$, $F' = 3$ manifold as a function of compensation power, showing a light-induced lifting of the degeneracy of the sublevels in addition to a linear mean shift. The zero-shift level is that of an atom free from both the trap and compensation lights. The three compensation intensities used repeatedly in the main text are shown, and the trap tone intensity matches that in the main text.

radial directions following an additional molasses stage after accumulation, and that the power-broadened linewidths in absence of any trap or compensation tone read 10 MHz for the utilized probe power. We find that the widths corresponding to the zero- and high-compensation powers show a more pronounced dependence on the radial temperatures (not shown) in comparison to the width corresponding to the intermediate compensation power where the mean shifts are canceled. This indicates that the spatial dispersion in the shifts are also a significant part of the observed widths unless the mean shift is canceled.

The combined effects of the tensor shifts and spatially broadened light shifts provide a picture that correctly reproduces the hierarchy of the linewidths observed in Fig. 2, albeit without an exact quantitative agreement. Nevertheless, further developing a model that can better predict the observed linewidths goes orthogonal to the scope of the current work, as the magnitude of the spread in the energy levels either due to the simulated tensor shifts or spread in the radial positions seem not to be relevant for capturing and cooling the atoms in the intracavity dipole trap given the relatively large effective detunings for the cooling light in the intracavity region—see main text.

APPENDIX C: SPIN-DEPENDENT CAVITY SHIFTS

We calibrate our fluorescence-based atom counting using the expected cavity shifts per spin flip given the well-characterized nature of the quantities that go into evaluating the atom-cavity coupling.

The quantization axis for the atoms in the dipole trap, defined by a 70-mG external magnetic field, is aligned parallel to the polarization of the 780-nm high-finesse cavity mode, coupling this mode to the atoms with π polarization. Focusing our attention on the two magnetically insensitive states $|F = 1, m_F = 0\rangle$ and $|F = 2, m_F = 0\rangle$ in the ground-state manifold, the cavity length is set such that the cavity mode couples these two states to the $5P_{3/2}$ excited-state manifold with opposite detunings of $\Delta = \pm 3.417$, corresponding to half the hyperfine splitting frequency. The effective interaction part of the Hamiltonian for this collective two-level system in this dispersive configuration is

$$\hat{H}_{\text{int}} = \hbar\Omega\hat{a}^\dagger\hat{a}\hat{J}_z, \tag{C1}$$

where $\Omega = 2g^2/\Delta$ is the dispersive frequency shift, $2g$ is the vacuum Rabi splitting, and $\hat{J}_z$ is the collective-spin population-difference operator [15,46]. As per Eq. (C1), the total cavity shift, detected by scanning a probe beam to find the reflection dip frequency, measures the population difference between the two hyperfine ground states. Given the cavity-mode parameters, the polarization, and the associated atomic transition matrix elements, the theoretical atom-cavity coupling rate and the cavity shift per spin flip are evaluated to be $g = 2\pi \times 85$ kHz and $\Omega/2\pi = 4.2$ Hz, respectively. The resulting single-atom cooperativity parameter is $C = 4g^2/\kappa\Gamma = 0.056$ for this high-finesse 780-nm traveling-wave mode. With $N = 4.0 \times 10^6$ atoms loaded into the dipole trap (see Appendix D), collective cooperativity can reach $NC = 2.2 \times 10^5$, putting the system deeply into the strong collective coupling regime.

For the atom-number calibration, after loading atoms into the dipole trap and further cooling, we state prepare them in the $|F = 1, m_F = 0\rangle$ ground state through optical pumping and a consecutive state-selective removal of the atoms from the trap with the push beam to purify the spin state. Following this state preparation, we observe 98.7%-contrast microwave-driven Rabi oscillations via fluorescence imaging. We calibrate the observed fluorescence signals using the independently measured cavity resonance shifts during the Rabi oscillations.

For the cavity shifts measured during continuous atom accumulation (Fig. 5), since the majority of atoms are observed to be in the $F = 1$ manifold, a 2-Hz/atom conversion factor can be taken as a guide to estimate the number of atoms located in the cavity mode. However, note that this is just a guide, since atoms are distributed across different magnetic manifolds, leading to different cavity couplings, and the exact spatial distributions of the atoms are not known during the loading procedure.

APPENDIX D: ALTERNATIVE LOADING SCHEMES

Here, we briefly mention a couple other loading variations we implemented that can optimize different quantities of interest.

First, we remark that even shallower traps can be utilized to continuously accumulate atoms, significantly relaxing the required laser powers compared to standard methods. This, in fact, optimizes for low temperatures with marginally reduced atom numbers. We have observed continuous accumulation in a 35-μK-deep trap (10 W), with atom numbers exceeding 1.5×10^6 at 5 μK axial and 9 μK radial temperatures in steady state. In this configuration, switching to traditional molasses cooling at the final phase of the protocol by optimally canceling the light shifts and turning off the MOT coils yields temperatures down to 3 μK.

For loading even more atoms into our usual 87-μK-deep trap, we have devised a loading scheme, albeit one that deviates from the purely steady-state operation principle. In this scheme, for the first 500 ms, we set the 1527-nm intracavity power to 2.8 W and MOT parameters to full power (see Appendix G). This allows the MOT to collect atoms as if in free space. Then, we apply a linear ramp of the 1527-nm power to 5.2 W in the last 50 ms. This results in 4×10^6 atoms (12% of the MOT) loaded into the dipole trap with axial and radial temperatures similar to those discussed in the main text. This constitutes the highest reported percentage of MOT to 1560-nm-dipole trap transfer efficiency. However, it shall be noted that higher efficiencies have previously been reported for other trap laser wavelengths [47,48]. Although this alternative method breaks the steady-state operation, the change in intracavity power is minimal: $\Delta P_{1527} = 2.5$ W in comparison to the 36-W trap power, leading to negligible photothermal effects.

APPENDIX E: OPTICAL CAVITY

The cavity mode has a single waist for all wavelengths involved in the setup, with waist values of 157, 155, and 111 μm for the 1560-, 1527-, and 780-nm modes, respectively, averaged over the two principal (sagittal and tangential) axes. The mode waists are colocated with the crossing region of the MOT beams (Fig. 1). The cavity spacer is built from Macor and the three attached mirrors forming an equilateral triangular mode with a circumference of 9.84 cm. The custom mirror coatings (Layertec) enhance the difference in the reflectivities of the two polarization modes, resulting in a high-finesse out-of-plane polarization mode (*s* polarization, FWHM linewidth, $\kappa_{1560,s} = 2\pi \times 30\,\text{kHz}$, $\kappa_{780,s} = 2\pi \times 85\,\text{kHz}$) and a low-finesse in-plane polarization mode (*p* polarization, $\kappa_{780,p} = 2\pi \times 1.39$ MHz). Note that in order to drive cavity-mediated Raman transitions, the cavity has to accommodate fundamental modes with perpendicular polarizations whose frequency offset matches the hyperfine splitting of ^{87}Rb. The polarization-dependent phase shifts from the specific mirror coatings also need to be taken into account for identification of the required cavity length to match this offset.

The residual scattering losses in the cavity mirrors can break the strict traveling-wave operation by backscattering light into counterpropagating cavity modes. In the presented experimental setup, we observe a typical backscattering fraction of 5×10^{-3} relative to the power in the primary 1560-nm high-finesse mode. The interference between the undesired counterpropagating tone and the primary tone is expected to yield a 14%-peak residual spatial intensity modulation along the cavity axis for the intracavity trap. Implications for future experiments and potential mitigation techniques are currently under investigation.

APPENDIX F: LASER SYSTEM FOR CAVITY INTERACTIONS

The 1560-nm source is a few-hertz-level linewidth external-cavity diode laser (OEwaves), the output of which is divided into three branches. The first branch is frequency doubled in a waveguide doubler (NTT) and coupled to a TEM_{00} high-finesse 780-nm mode to serve as the cavity probe beam in this work. The second branch is coupled to a TEM_{00} high-finesse 1560-nm mode after it passes through an electro-optic I/Q modulator in carrier-suppressed single-sideband mode (SSB) [49] to form the dipole trap. This modulator, operated at 228 MHz, is used for shifting the frequency of the 780-nm tone relative to the 1560-nm mode to compensate for the difference in the effective cavity lengths for the two wavelengths. This configuration ensures simultaneous resonance of the dipole trap tone and the 780-nm tone. The third branch, although not utilized in this work, passes through another SSB modulator with a 3.417-GHz shift, after which it is frequency doubled to serve as one of the future Raman beams, coupled to the low-finesse 780-nm TEM_{00} mode. In the context of Raman transitions, the probe beam serves as the second arm, completing the two-photon transition. Finally, the light-shift compensation tone is obtained from a separate 1527-nm fiber laser (NP-Photonics) with a linewidth of 500 Hz. This light is directly coupled to a 1527-nm counterpropagating low-finesse TEM_{00} mode.

We use squash lock [11] for the 1560-nm laser-cavity frequency stabilization, and additionally stabilize the intracavity power by monitoring the cavity transmission to achieve a low-noise trapping potential. Squash lock is a modulation-free approach which uses a quadrant photodiode (QPD) to derive an error signal from changes in beam-shape ellipticity in cavity reflection. The cylindrical lens pair shown in Fig. 1 is used for beam shaping, which is crucial for this method. The analog error signal is filtered [50] and distributed to three feedback channels: High-frequency noise is suppressed by feedback to the 1560-nm laser, which is simultaneously keyed to a ^{85}Rb transition via a low-bandwidth offset lock. Low-frequency drifts (<10 Hz) and structural resonances (~3.5 kHz) are suppressed via feedback to the linear stage and ring piezo, respectively.

APPENDIX G: LASER SYSTEM FOR MOT

The MOT laser system generates the cooling and repump tones addressing the $|5S_{1/2}, F = 2\rangle \leftrightarrow |5P_{3/2}, F' = 3\rangle$ and $|5S_{1/2}, F = 1\rangle \leftrightarrow |5P_{3/2}, F' = 2\rangle$ transitions of ^{87}Rb [42]. These tones are derived from 780-nm external-cavity diode lasers (Sacher) and are frequency-offset locked [51] to a reference laser that is itself locked to the ^{85}Rb transition $|5S_{1/2}, F = 3\rangle \leftrightarrow |5P_{3/2}, F' = 4\rangle$ via modulation-transfer spectroscopy [52]. In typical operating conditions, each of the three pairs of counterpropagating MOT cooling beams has an intensity of 10 mW/cm^2 with a spot size of 0.8 cm and a red-detuning of $-2.5\,\Gamma$. There is a single beam for the repump tone with an intensity of 5 mW/cm^2 with a spot size of 0.8 cm. The magnetic field gradient for the MOT is 10 G/cm. A 2D-MOT-based atom source (Cold Quanta) delivers rubidium atoms into the science chamber through a pinhole. The loading location of the MOT is aligned with the cavity mode waist and can be adjusted within a couple of millimeters through external magnetic bias fields. In typical operating conditions, the MOT loads at a rate of 6×10^7 atoms/s and maintains the loaded atoms at temperatures around 300 μK, as indicated by time-of-flight measurements.

We measure the $1/e$ lifetime of the MOT to be 5.4 s. Fluorescence imaging (FLIR Blackfly CMOS camera) is used to determine the atom numbers and temperatures. The conversion of detected counts to atom numbers for the fluorescence based atom number calibration can be done as in Ref. [42]. However, for this atom number calibration, we use a cavity-based calibration method, more suited for our application; see Appendix C.

APPENDIX H: ADDITIONAL PERIPHERALS

A microwave antenna is integrated inside the vacuum chamber in the form of a $\lambda/4$ dipole antenna that is directly attached to an SMA vacuum feedthrough. The antenna is used for coherent manipulation of the atomic state between the ^{87}Rb magnetically insensitive hyperfine clock states, separated by 6.834 GHz. For driving this antenna, a 7.2-GHz ultralow-noise microwave source (Wenzel Associates) is frequency mixed with an agile direct digital synthesizer (AD9910) operated at 366 MHz. The Rabi oscillation rate induced by this source is $\Omega_R/2\pi = 3.8$ kHz with 28 dBm of input microwave power. This spectroscopic tool is utilized, for example, for zeroing the magnetic fields at specific instances in this work by observing the magnetic Zeeman shifts on the ground-state sublevels.

For the atomic-state preparation, we optically pump the atoms into the magnetically insensitive $|F = 1, m_F = 0\rangle$ state. This is achieved by driving the atoms with a π-polarized repump tone tuned to the $|5S_{1/2}, F = 1\rangle \leftrightarrow |5P_{3/2}, F' = 1\rangle$ transition, while the cooling light is tuned to the $|5S_{1/2}, F = 2\rangle \leftrightarrow |5P_{3/2}, F' = 2\rangle$. In this configuration, the $|F = 1, m_F = 0\rangle$ state is a dark state due to the selection rules, where the atoms accumulate [53,54].

The experimental sequences are controlled through the ARTIQ Hardware using the Quantrol open-source graphical user interface developed in our group [55].

[1] V. M. Schäfer, Z. Niu, J. R. Cline, D. J. Young, E. Y. Song, H. Ritsch, and J. K. Thompson, Continuous recoil-driven lasing and cavity frequency pinning with laser-cooled atoms, Nat. Phys. **21**, 902 (2025).

[2] J. R. Cline, V. M. Schäfer, Z. Niu, D. J. Young, T. H. Yoon, and J. K. Thompson, Continuous collective strong coupling of strontium atoms to a high finesse ring cavity, Phys. Rev. Lett. **134**, 013403 (2025).

[3] K. Singh, S. Anand, A. Pocklington, J. T. Kemp, and H. Bernien, Dual-element, two-dimensional atom array with continuous-mode operation, Phys. Rev. X **12**, 011040 (2022).

[4] C.-C. Chen, R. González Escudero, J. Minář, B. Pasquiou, S. Bennetts, and F. Schreck, Continuous Bose–Einstein condensation, Nature (London) **606**, 683 (2022).

[5] J. M. Kwolek and A. T. Black, Continuous sub-Doppler-cooled atomic beam interferometer for inertial sensing, Phys. Rev. Appl. **17**, 024061 (2022).

[6] M. Schioppo, R. C. Brown, W. F. McGrew, N. Hinkley, R. J. Fasano, K. Beloy, T. Yoon, G. Milani, D. Nicolodi, J. Sherman, *et al.*, Ultrastable optical clock with two cold-atom ensembles, Nat. Photon. **11**, 48 (2017).

[7] H. Krauter, C. A. Muschik, K. Jensen, W. Wasilewski, J. M. Petersen, J. I. Cirac, and E. S. Polzik, Entanglement generated by dissipation and steady state entanglement of two macroscopic objects, Phys. Rev. Lett. **107**, 080503 (2011).

[8] J. T. Reilly, S. B. Jäger, J. Cooper, and M. J. Holland, Fully collective superradiant lasing with vanishing sensitivity to cavity length vibrations, Phys. Rev. Lett. **136**, 143803 (2026).

[9] T. M. Karg, B. Gouraud, C. T. Ngai, G.-L. Schmid, K. Hammerer, and P. Treutlein, Light-mediated strong coupling between a mechanical oscillator and atomic spins 1 meter apart, Science **369**, 174 (2020).

[10] J. A. Muniz, D. Crow, H. Kim, J. M. Kindem, W. B. Cairncross, A. Ryou, T. C. Bohdanowicz, C.-A. Chen, Y. Ji, A. W. M. Jones, *et al.*, Repeated ancilla reuse for logical computation on a neutral atom quantum computer, Phys. Rev. X **15**, 041040 (2025).

[11] F. Diorico, A. Zhutov, and O. Hosten, Laser-cavity locking utilizing beam ellipticity: Accessing the 10-7 instability scale relative to cavity linewidth, Optica **11**, 26 (2024).

[12] L. Pezze, A. Smerzi, M. K. Oberthaler, R. Schmied, and P. Treutlein, Quantum metrology with nonclassical states of atomic ensembles, Rev. Mod. Phys. **90**, 035005 (2018).

[13] S. S. Szigeti, O. Hosten, and S. A. Haine, Improving cold-atom sensors with quantum entanglement: Prospects and challenges, Appl. Phys. Lett. **118**, 140501 (2021).

[14] M. Kitagawa and M. Ueda, Squeezed spin states, Phys. Rev. A **47**, 5138 (1993).

[15] M. H. Schleier-Smith, I. D. Leroux, and V. Vuletić, Squeezing the collective spin of a dilute atomic ensemble by cavity feedback, Phys. Rev. A **81**, 021804(R) (2010).

[16] K. C. Cox, G. P. Greve, J. M. Weiner, and J. K. Thompson, Deterministic squeezed states with collective measurements and feedback, Phys. Rev. Lett. **116**, 093602 (2016).

[17] O. Hosten, N. J. Engelsen, R. Krishnakumar, and M. A. Kasevich, Measurement noise 100 times lower than the quantum-projection limit using entangled atoms, Nature (London) **529**, 505 (2016).

[18] O. Hosten, R. Krishnakumar, N. J. Engelsen, and M. A. Kasevich, Quantum phase magnification, Science **352**, 1552 (2016).

[19] B. K. Malia, Y. Wu, J. Martínez-Rincón, and M. A. Kasevich, Distributed quantum sensing with mode-entangled spin-squeezed atomic states, Nature (London) **612**, 661 (2022).

[20] G. P. Greve, C. Luo, B. Wu, and J. K. Thompson, Entanglement-enhanced matter-wave interferometry in a high-finesse cavity, Nature (London) **610**, 472 (2022).

[21] C. Cassens, B. Meyer-Hoppe, E. Rasel, and C. Klempt, Entanglement-enhanced atomic gravimeter, Phys. Rev. X **15**, 011029 (2025).

[22] A. D. Cronin, J. Schmiedmayer, and D. E. Pritchard, Optics and interferometry with atoms and molecules, Rev. Mod. Phys. **81**, 1051 (2009).

[23] C. F. Ockeloen, R. Schmied, M. F. Riedel, and P. Treutlein, Quantum metrology with a scanning probe atom interferometer, Phys. Rev. Lett. **111**, 143001 (2013).

[24] A. Peters, K. Y. Chung, and S. Chu, Measurement of gravitational acceleration by dropping atoms, Nature (London) **400**, 849 (1999).

[25] M. Kasevich and S. Chu, Atomic interferometry using stimulated Raman transitions, Phys. Rev. Lett. **67**, 181 (1991).

[26] A. Aeppli, K. Kim, W. Warfield, M. S. Safronova, and J. Ye, Clock with 8×10^{-19} systematic uncertainty, Phys. Rev. Lett. **133**, 023401 (2024).

[27] E. Pedrozo-Peñafiel, S. Colombo, C. Shu, A. F. Adiyatullin, Z. Li, E. Mendez, B. Braverman, A. Kawasaki, D. Akamatsu, Y. Xiao, *et al.*, Entanglement on an optical atomic-clock transition, Nature (London) **588**, 414 (2020).

[28] N. J. Engelsen, Quantum metrology using large ensembles of entangled atoms, Ph.D. thesis, Stanford University, 2016.

[29] D. S. Naik, H. Eneriz-Imaz, M. Carey, T. Freegarde, F. Minardi, B. Battelier, P. Bouyer, and A. Bertoldi, Loading and cooling in an optical trap via hyperfine dark states, Phys. Rev. Res. **2**, 013212 (2020).

[30] G. Kuyumjyan, Condensation de Bose-Einstein multiple dans les modes d'ordre supérieurs d'une cavité optique bi-fréquence, Ph.D. thesis, Université de Bordeaux, 2017.

[31] P. Griffin, K. Weatherill, S. MacLeod, R. Potvliege, and C. Adams, Spatially selective loading of an optical lattice by light-shift engineering using an auxiliary laser field, New J. Phys. **8**, 11 (2006).

[32] S. Coop, S. Palacios, P. Gomez, Y. N. M. de Escobar, T. Vanderbruggen, and M. W. Mitchell, Floquet theory for atomic light-shift engineering with near-resonant polychromatic fields, Opt. Express **25**, 32550 (2017).

[33] S. Palacios, S. Coop, P. Gomez, T. Vanderbruggen, Y. N. M. de Escobar, M. Jasperse, and M. W. Mitchell, Multi-second magnetic coherence in a single domain spinor Bose–Einstein condensate, New J. Phys. **20**, 053008 (2018).

[34] T. Vanderbruggen, R. Kohlhaas, A. Bertoldi, S. Bernon, A. Aspect, A. Landragin, and P. Bouyer, Feedback control of trapped coherent atomic ensembles, Phys. Rev. Lett. **110**, 210503 (2013).

[35] R. Kohlhaas, A. Bertoldi, E. Cantin, A. Aspect, A. Landragin, and P. Bouyer, Phase locking a clock oscillator to a coherent atomic ensemble, Phys. Rev. X **5**, 021011 (2015).

[36] D. Bluvstein, A. A. Geim, S. H. Li, S. J. Evered, J. P. B. Ataides, G. Baranes, A. Gu, T. Manovitz, M. Xu, M. Kalinowski, *et al.*, A fault-tolerant neutral-atom architecture for universal quantum computation, Nature (London) **649**, 39 (2026).

[37] H. J. Metcalf and P. Van der Straten, *Laser Cooling and Trapping* (Springer Science & Business Media, Berlin/Heidelberg, 1999).

[38] B. Arora, M. S. Safronova, and C. W. Clark, Magic wavelengths for the *np-ns* transitions in alkali-metal atoms, Phys. Rev. A **76**, 052509 (2007).

[39] S. Bernon, Trapping and nondemolition measurement of cold atoms in a high-finesse ring cavity, Ph.D. thesis, Ecole Polytechnique, Palaiseau, France, 2011.

[40] J.-P. Brantut, J.-F. Clément, M. R. de Saint Vincent, G. Varoquaux, R. A. Nyman, A. Aspect, T. Bourdel, and P. Bouyer, Light-shift tomography in an optical-dipole trap for neutral atoms, Phys. Rev. A **78**, 031401(R) (2008).

[41] C.-Y. Shih and M. S. Chapman, Nondestructive light-shift measurements of single atoms in optical dipole traps, Phys. Rev. A **87**, 063408 (2013).

[42] D. A. Steck, Rubidium 87 D line data (2001) http://steck.us/alkalidata.

[43] S. Chu, L. Hollberg, J. E. Bjorkholm, A. Cable, and A. Ashkin, Three-dimensional viscous confinement and cooling of atoms by resonance radiation pressure, Phys. Rev. Lett. **55**, 48 (1985).

[44] C. Adams and E. Riis, Laser cooling and trapping of neutral atoms, Prog. Quantum Electron. **21**, 1 (1997).

[45] M. S. Safronova and U. I. Safronova, Critically evaluated theoretical energies, lifetimes, hyperfine constants, and multipole polarizabilities in ^{87}Rb, Phys. Rev. A **83**, 052508 (2011).

[46] K. Hammerer, K. Mølmer, E. S. Polzik, and J. I. Cirac, Light-matter quantum interface, Phys. Rev. A **70**, 044304 (2004).

[47] S. J. M. Kuppens, K. L. Corwin, K. W. Miller, T. E. Chupp, and C. E. Wieman, Loading an optical dipole trap, Phys. Rev. A **62**, 013406 (2000).

[48] K. Brzozowski, L. Krzemien, J. Zachorowski, and W. Gawlik, Diagnostics and loading of an atomic optical dipole trap, Optica Applicata **40**, 557 (2010).

[49] S. Wald, F. Diorico, and O. Hosten, Analog stabilization of an electro-optic I/Q modulator with an auxiliary modulation tone, Appl. Opt. **62**, 1 (2023).

[50] R. W. Fox, C. W. Oates, and L. W. Hollberg, 1. Stabilizing diode lasers to high-finesse cavities, in *Experimental Methods in the Physical Sciences* (Elsevier, New York, 2003), Vol. 40, pp. 1–46.

[51] V. Li, F. Diorico, and O. Hosten, Laser frequency-offset locking at 10-Hz-level instability using hybrid electronic filters, Phys. Rev. Appl. **17**, 054031 (2022).

[52] R. K. Raj, D. Bloch, J. J. Snyder, G. Camy, and M. Ducloy, High-frequency optically heterodyned saturation spectroscopy via resonant degenerate four-wave mixing, Phys. Rev. Lett. **44**, 1251 (1980).

[53] G. Avila, V. Giordano, V. Candelier, E. de Clercq, G. Theobald, and P. Cerez, State selection in a cesium beam by laser-diode optical pumping, Phys. Rev. A **36**, 3719 (1987).

[54] Y.-X. Duan, B. Wang, J.-F. Xiang, Q. Liu, Q.-Z. Qu, D.-S. Lü, and L. Liu, State preparation in a cold atom clock by optical pumping, Chin. Phys. Lett. **34**, 073201 (2017).

[55] https://github.com/hostengroup.